I. MANIA[1*], H. PAUL[1], R. CHULIST[1], P. PETRZAK[1], M. MISZCZYK[1], M. PRAŻMOWSKI[2]

CRYSTAL LATTICE ROTATIONS INDUCED BY SHEAR BANDING IN FCC METALS DEFORMED AT HIGH STRAIN RATES

In this paper, the microstructural and texture changes in polycrystalline CuZn30 alloy, copper, and AA1050 aluminium alloy have been studied to describe the crystal lattice rotation during shear bands formation. The hat-shaped specimens were deformed using a drop-hammer at the strain rate of 560 s^{-1}. Microstructure evolution was investigated using optical microscopy, whereas texture changes were examined with the use of a scanning electron microscope equipped with the EBSD facility. The microstructural observations were correlated with nanohardness measurements to evaluate the mechanical properties of the sheared regions. The analyses demonstrate the gradual nature of the shear banding process, which can be described as a mechanism of the bands nucleation and then successive growth rather than as an abrupt instability. It was found that regardless of the initial orientation of the grains inside the sheared region, a well-defined tendency of the crystal lattice rotation is observed. This rotation mechanism leads to the formation of specific texture components of the sheared region, different from the one observed in a weakly or non-deformed matrix. During the process of rotation, one of the {111} planes in each grain of the sheared region 'tends' to overlap with the plane of maximum shear stresses and one of the <110> or <112> directions align with the shear direction. This allows slip propagation through the boundaries between adjacent grains without apparent change in the shear direction. Finally, in order to trace the rotation path, transforming the matrix texture components into shear band, rotation axis and angles were identified.

Keywords: shear bands; high strain rates; texture; SEM/EBSD

1. Introduction

Shear banding is a mechanism of strain localization that occurs in the majority of metallic materials deformed in the range of large strains. Since a significant part of the plastic deformation work is converted into heat, it is clear that strain rate has to strongly determine the 'rate' of the heat generation and dissipation in the system. According to the rate of heat generation/dissipation, two types of shear bands (SB), namely, (i) *isothermal shear bands (ISBs)* and (ii) *adiabatic shear bands (ASBs)* [1] are distinguished. ISBs are formed during (semi) static straining [2], i.e. under 'conventional' strain rates, when the heat generation rate is significantly lower than the rate of energy dissipation. Thus, the temperature of the system may be assumed to be unaltered. The ASB's are formed under high and extremely high strain rates. In that case, the shear localization can be regarded as an adiabatic process because the heat within the narrow SB area is hard to diffuse in an extremely short time. This results in a rapid local increase of temperature and leads to

the 'thermal softening' of material [3] along the band line. The formation of macro-/micro- scale ASB is often associated with the presence of geometrical or microstructural defects [4]. It is a signal of reduction or complete loss of deformation ability and is considered as an important precursor to material failure [5] and dramatic degradation of the load-bearing properties of the metallic parts. Therefore, it is typically considered to be detrimental to the strength of materials.

However, the elementary mechanism responsible for ASB nucleation, thickening, and propagation across the grain boundaries is still relatively limited, despite a strong interest in the shear banding in poly- and single-crystalline metals. To date, a significant part of the literature that describes the mechanism of SB formation in the range of very high strain rates, links their appearance to heat dissipation and dynamic recrystallization [6-10]. The leading paradigm is that competition between strain hardening (due to severe plastic deformation) and thermal softening (due to sharp temperature rise) determines the initiation of the bands and the onset of failure. Hence, a large number

[1] POLISH ACADEMY OF SCIENCES, INSTITUTE OF METALLURGY AND MATERIALS SCIENCE, 25 REYMONTA STR., 30-059 KRAKOW, POLAND
[2] OPOLE UNIVERSITY OF TECHNOLOGY, FACULTY OF MECHANICS, 76 PRÓSZKOWSKA STR., 45-758 OPOLE, POLAND

* Corresponding author: i.mania@imim.pl

320

of works were focused on the criteria of SB nucleation [11,12], the structure evolution due to phase transformation [8,13], and the mechanisms of strain hardening and recrystallization [6,14]. This description of the phenomenon, based on the mechanism originally proposed by Zener and Hollomon [1] assumes a destabilizing effect of thermal softening of the material, in which the plastic work is converted into heat to a significant extent. Thermal softening begins to dominate over strain hardening in given areas, especially in materials of low thermal conductivity [7,15-17]. This results in a sudden strain localization. Another group of works is based on the assumption that the occurrence of SB at high strain rates is related to dynamic recrystallization [5,10]. This is due to the observation that ASB formation is typically promoted by the low thermal conductivity of metals, [9,10,18-20], where a local increase of temperature leads to the formation of dynamically recrystallized grains and then to local 'softening' of the adjacent structure and the band nucleation. However, the above descriptions of the mechanisms of ASB formation contains some gaps:

- The first group of problems is related to the role of temperature rise during the process. A large amount of plastic deformation leads to a strong increase in the energy stored in an ASB area. Experiments focused on the evaluation of temperature rise during the shearing process, e.g. [10,21,22] revealed that temperature rise and ASB formation occur simultaneously, but clear evidence of their causal relationship was not defined. In metals of low thermal conductivity, temperature rise increases the ability of the structure to dynamic recrystallization (even at room temperature). This leads to the conclusion that new recrystallized grains' appearance inside the ASB area is a 'secondary effect' since the new grains are formed by recrystallization of strongly deformed areas.
- Another aspect is related to the link between morphological changes and changes in the orientation of the crystal lattice during the band formation. In accordance with the model proposed to explain the mechanism of SB formation in materials deformed at 'conventional' strain rates, the initial

stages of this process are associated with local, but strictly defined re-orientation of the crystal lattice in the narrow areas [23,24]. In fcc metals, this process leads to the formation of specific texture components within the SB, different from those identified in the surrounding, less deformed matrix. This allows crystallographic slip propagation in the neighbouring grains along the macroscopically observed shear band plane, with no apparent change in slip direction.

However, during high-speed deformation, the SB forms also in metals of good thermal conductivity. This shows that the thermal conductivity of the material is not the decisive factor, or at least not the only factor, that decides for the nucleation of SB. The present work was aimed at tracing the exact 'rotation path' of the crystal lattice in face-centered cubic (fcc) metals deformed at high strain rates. Due to the axial geometry of specimens, well-defined SB demonstrating specific texture components were formed during displacement of the upper part of hat-shaped specimen (hat) towards the bottom one (brim). To capture texture changes corresponding to SB formation electron backscatter diffraction (EBSD) in a scanning electron MICROSCOPE (SEM) was used.

2. Experimental

Hat-shaped specimens cut-off from hot-rolled aluminium (AA1050) described here as Al, extruded copper (Cu-ETP) described here as Cu, and CuZn30 alloy described here as Br were selected for the experiment. An axial geometry of specimens (Fig. 1a) contributes to the tendency of shear to appear in narrow areas even in materials that do not tend to localize strain easily. In the case of Al, the specimens were cut-off so that the principal axis of the hat-shaped specimen (axial direction – AD) coincided with the normal direction (ND) of the hot-rolled sheet (Fig. 1b). In the case of Cu and Br, the AD of the hat-shaped samples coincided with the extrusion direction (ED) (Fig. 1c).
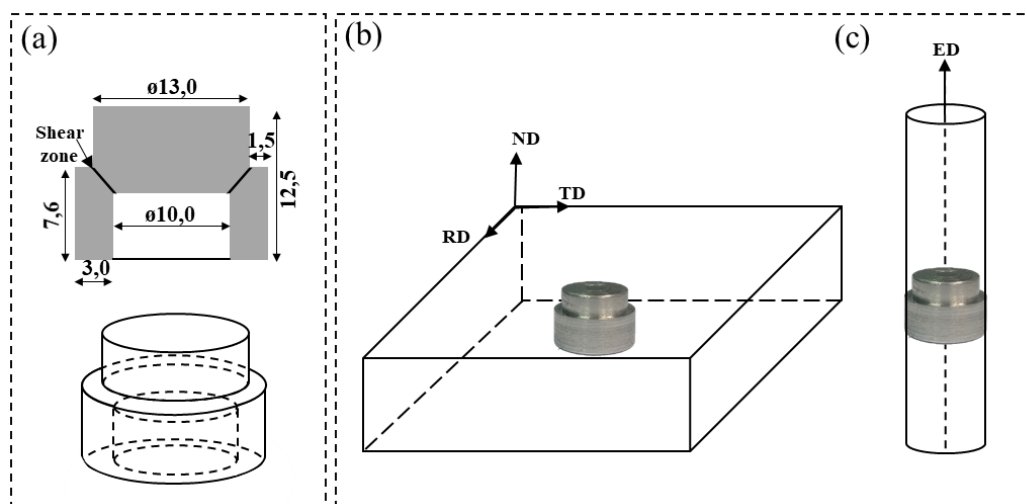

Fig. 1. (a) Typical hat-shaped specimen dimension in millimetres and specimen orientation as machined from (b) the hot-rolled plate (AA1050 alloy – Al) and (c) the extruded rods (Cu and CuZn30 alloy – Br)

For the initial materials, orientation maps were measured on two mutually perpendicular sections: in the case of Al on cross-sections perpendicular to rolling and transverse directions, whereas in the case of Cu and Br on the longitudinal section, i.e., parallel to the ED and on the transverse section, i.e. in the section perpendicular to ED. For post-processed hat-shaped specimens, morphological and textural analyses were conducted on the axial cross-section, whereas the texture components were analysed in the reference system associated with the axial (AD) and radial (RD) directions. The deformation process was carried out with the use of drop-hammer – Instron Ceast 9350, under applied energy of 600 J and strain rate of $560 \, s^{-1}$. To obtain assumed strain, the 'stop rings' were applied during the process. Macro-scale morphological changes were analysed using optical microscopy (OM) on etched specimens. In order to reveal the microstructure for OM observation, Al specimen was electropolished prior to electrolytic anodising using a 3% HBF4 solution. Cu and Br samples, after mechanical polishing on 7000 SiC papers, were etched with the use of Chromium and Nital (HNO_3 in C_2H_5OH) solutions, respectively.

More detailed microstructural and textural analyses of the initial and as-deformed materials were carried out using SEM – FEI Quanta 3D operating at 15-20 kV and equipped with an EBSD facility. The step sizes applied during the acquisition of the orientation maps ranged between 50 nm and 900 nm. Very low step sizes (<100 nm) were applied to reveal details of the microstructural features, whereas larger step sizes (>100 nm) were applied to capture textural changes during the matrix incorporation into the macro- SB area. The binning size applied for data acquisition was 4×4. Software used for EBSD analysis was TSL OIM Analysis. The pole figures were calculated with Harmonic Series Expansion method (Gaussian Half-Width of 0.2). Grain dilatation was applied as cleaning criterion for EBSD map. For the purpose of determination of strain hardening after hammering, nano-hardness tests were carried out with the use of Nanoindenter G200 AGILENT and Fisher Pikodentor HM500.

3. Results and discussion

3.1. Initial microstructure and texture

AA1050 alloy. The initial microstructure of the Al sheet (Fig. 1a) is composed of flattened grains with dimensions in the rolling and transverse directions of several hundred microns. The grains thickness, i.e., dimension in the ND direction was in the range of 20-60 μm. In ongoing research, the boundaries of these flattened grains provide excellent markers to analyse the morphological aspects of SB formation due to displacement of the upper part of the hat to the inside of the brim. The initial texture of the Al sheet was described by components typically observed in hot-rolled Al-based alloy sheets/plates, i.e. two variants of brass{110}<112> orientations with scattering towards four variants of the S{123}<634> (Fig. 2a). The lack of two variants of C{112}<111> orientation, which are typically observed in strongly deformed face centred cubic (*fcc*) metals of high stacking fault energy (SFE) is associated with a well-defined representation of cube{100}<001> orientation, due to development of a significant fraction of fully recrystallized cube-oriented grains.

Copper and CuZn30 alloy. In the case of Cu (Fig. 2b) and Br (Fig. 2c), the initial materials consisted of equiaxed grains (as documented by SEM/EBSD observation in two perpendicu-
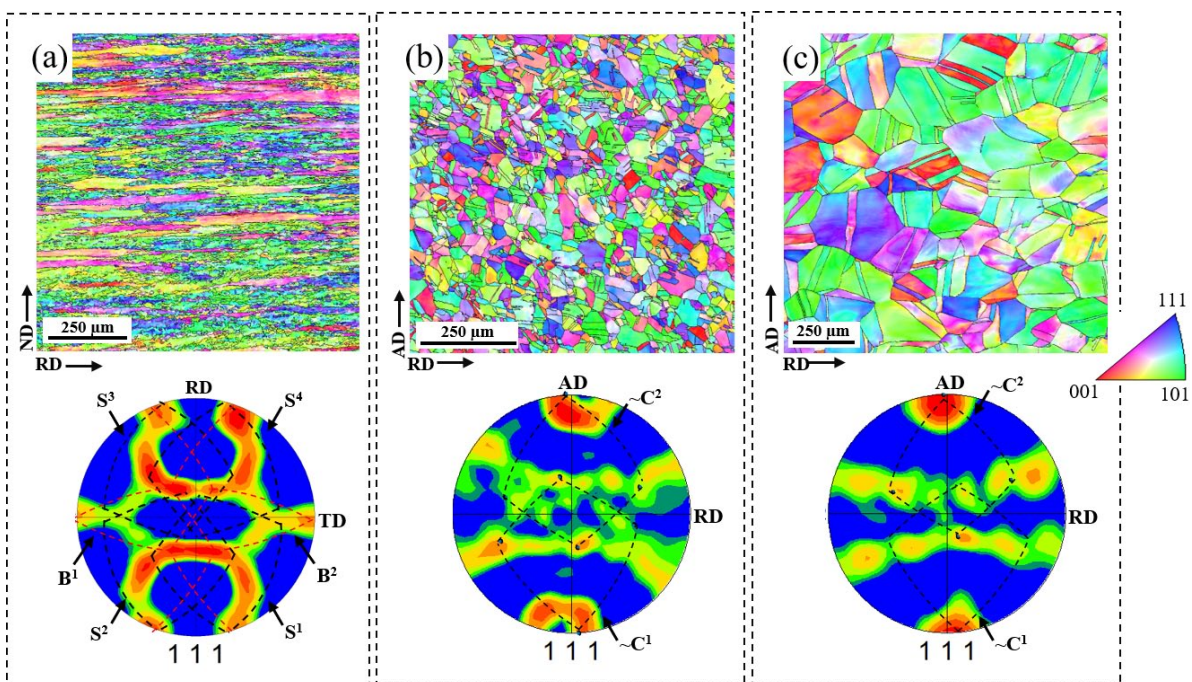

Fig. 2. Microstructure and texture of as-received materials: (a) Al, (b) Cu, and (c) Br. SEM/EBSD orientation maps presented using IPF colour code combined with high angle boundaries (>15º) and corresponding the {111} pole figures.. The dashed lines indicate the relevant texture components, where S – {123}<634>, Brass (B) – {110}<112>, C – {112}<111>

lar sections) with an average diameter of 40 mm and 150 mm for Cu and Br, respectively. After the extrusion, both materials exhibited a <111> and <100> double fiber texture, as analysed in axial and perpendicular to ED sections.

3.2. Macro-scale morphological changes in shear band region

The specific shape of the specimens determines the character of the shear surface. The displacement of the upper part of the hat into the interior of its lower part results in shearing along the surface, which in 3D is the lateral surface of the sheared cone. This specific character of the shear surface (resulting from the axial symmetry of the deformed specimen) causes that the SB observed on both sides of axial sections of the specimen are essentially the same microstructural elements, but mirror-reflected. Thus only one macro- SB (right or left) was analysed in each case.

To a first approximation, optical microscopy was applied to examine the macroscopically observed structural features of the SB on axial sections of the hat-shaped specimens. After deformation, the original structure of the hot-rolled and extruded samples has changed in the sheared regions, where forced shear stresses concentrate. Figs 3a-c show the microstructure of the sheared regions and their adjacent areas for Al (a), Cu (b), and Br (c), between the upper and lower corners. It is clear that the degree of strain localization depends on the metal analysed, whereas the width of the sheared region varies strongly along the shear band line. The areas of most intense shear are located near both corners

(near free surfaces) and propagate towards the inner regions of the sample. The widths of the SB gradually narrow down along the shear direction from the middle to the bottom or to a less degree from the middle to top layers of the sample. This leads to the conclusion that the SB are initiated near the free surfaces of the specimens, where the shear localization is greatest, and then propagate towards inner regions of the sample. In Al and Cu, the forming SB are 'dispersed', while in the Br specimen the SB is much more localized.

Effect of displacement of the upper part of the hat is particularly well-observed in Al samples. Since the initial structure of Al in sections parallel to the main sample axis is composed of flattened grains with the grain boundaries situated perpendicular to the main axis of the hat-shaped specimen, these boundaries can be used as specific markers of the morphological changes during SB formation. In the sheared area, the inclination of the flattened grains fragments (in fact their boundaries) is changed *via* rotation that leads to the decrease of inclination of longer grain axes in relation to the main sample axis. The rotation angle of the flattened grains changes when moving from the matrix areas to the SB core areas. However, the magnitude of these changes is strongly dependent on the location of the analysed area along the band length; it is greatest in the areas near the free surfaces and decreases in the middle parts. A detailed analysis of the grain boundaries inclination carried out in the band shows a change from 0° (matrix) to 80°-85° in the band core. The mechanism of kink-type bands formation as a precursor of well-developed SB during matrix incorporation into the band area assumes that pile-up of dislocations in the vicinity of the potential shear
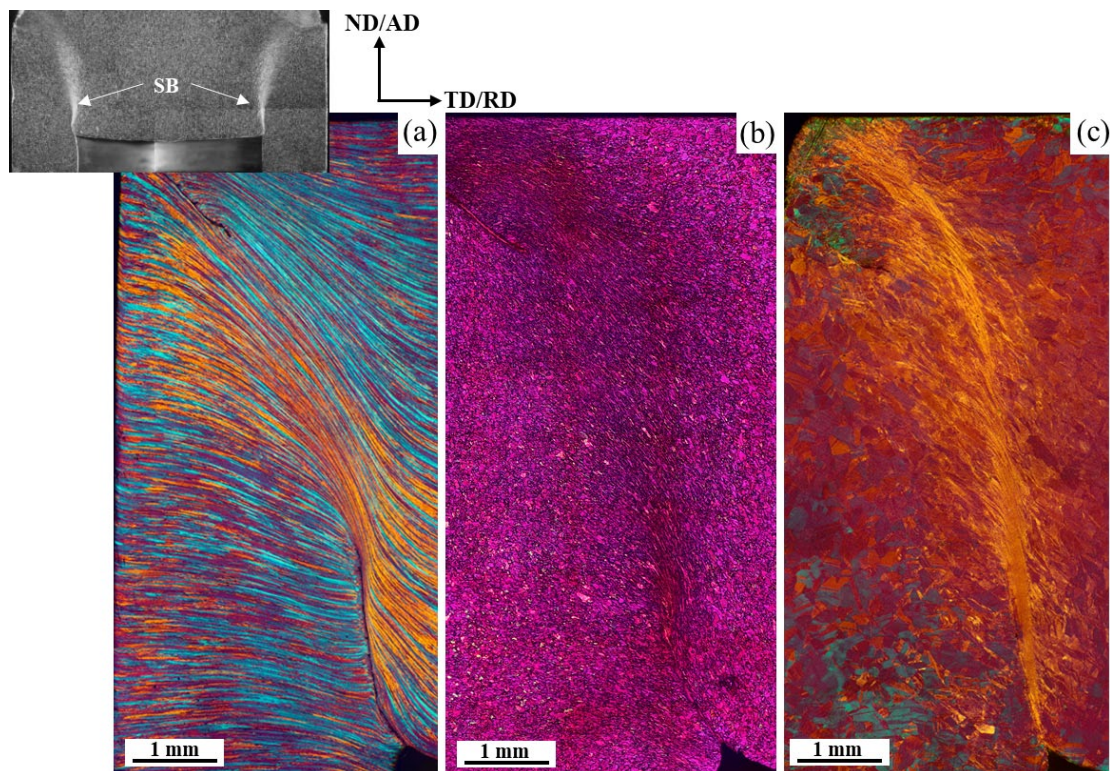

Fig. 3. Macroscopic SB developed in hat-shaped specimens deformed at the strain rate of 560 s^{-1} in (a) Al, (b) Cu, and (c) Br. Optical microscopy observation in polarized light. Axial sections

bands leads to a strictly defined rotation of the crystal lattice. As a result, the elements of the structure are gradually situated parallel to the shear direction [25].

In the case of Cu and Br, the regions of strongest strain localization are formed near the bottom free surfaces, while the upper part is much more diffuse. Near the core of the band, only severely deformed and flattened grains are observed. The structure of the material lying away from the core of the band consists of the equiaxed grains, whereas the matrix is practically non-deformed. In the case of Br, the degree of strain localisation is much greater, as compared to Al and Cu, particularly near the lower free surface. In this area, the band forms a straight line along with a large distance of the analysed cross-section. The structure of the band interior in these areas is extremely refined. Areas of less localized deformation reveal the formation of a structure of strongly flattened grains, for which the position of the longer axis approaches the shear direction.

3.3. Orientation changes resulting from the shear band formation

For as-deformed samples, all orientation maps presented in this study use the inverse pole figure (IPF) colouring code in which the red, blue and green colour represents <001>, <011>, and <111> direction, respectively. In some cases, the IPF maps

were combined with the image quality factor. Orientation maps were received from the central (axial) part of the samples corresponding to the non-deformed (or only slightly deformed) matrix as well as from the left or right SB region to capture texture image differences; this opens the possibility to determine the mechanism responsible for the SB formation. It was found that the orientations of the matrix undergo differentiated, but not accidental rotation during the matrix incorporation into the macro-SB area. However, strongly rotated grains in the band region are always located near the free surfaces, where one of the <110> crystallographic directions situates parallel to the shear direction.

For the Al sample (Fig. 4) measured texture of the matrix consisted of three main groups of orientations, which are defined as: $(Al)M^1 – (–110)[–1 –12]$, $(Al)M^2 – (04 –3)[–535]$, and (Al) $M^3 – (–110)[–5 –5 –2]$, as shown in the {111} pole figure of Fig. 4c. The groups of orientations present in the SB area were identified as: $(Al)MSB^{R1} – (–110)[–1 –13]$ and $(Al)MSB^{R2} – (02 –3)[–532]$ (Fig. 4d-e). An analogic procedure was applied for Cu specimens (Fig. 5). As presented on {111} pole figure (Fig. 5c) the non-deformed matrix of Cu was described by two main groups of orientations: $(Cu)M^1 – (2 1 4)[–10 –8 7]$ and $(Cu)M^2 – (–1 3 –2)[–8 –6 –5]$. Two main texture components were measured inside the macro-SB area (Fig. 5d-e), which were identified as: $(Cu)MSB^{L1} (6 5 –1)[6 –7 1]$ and $(Cu)MSB^{L2}$ $(1 1 –1)[–6 7 1]$. The initial texture 'image' of Br (Fig. 6 c) was composed of two groups of components, that can be described
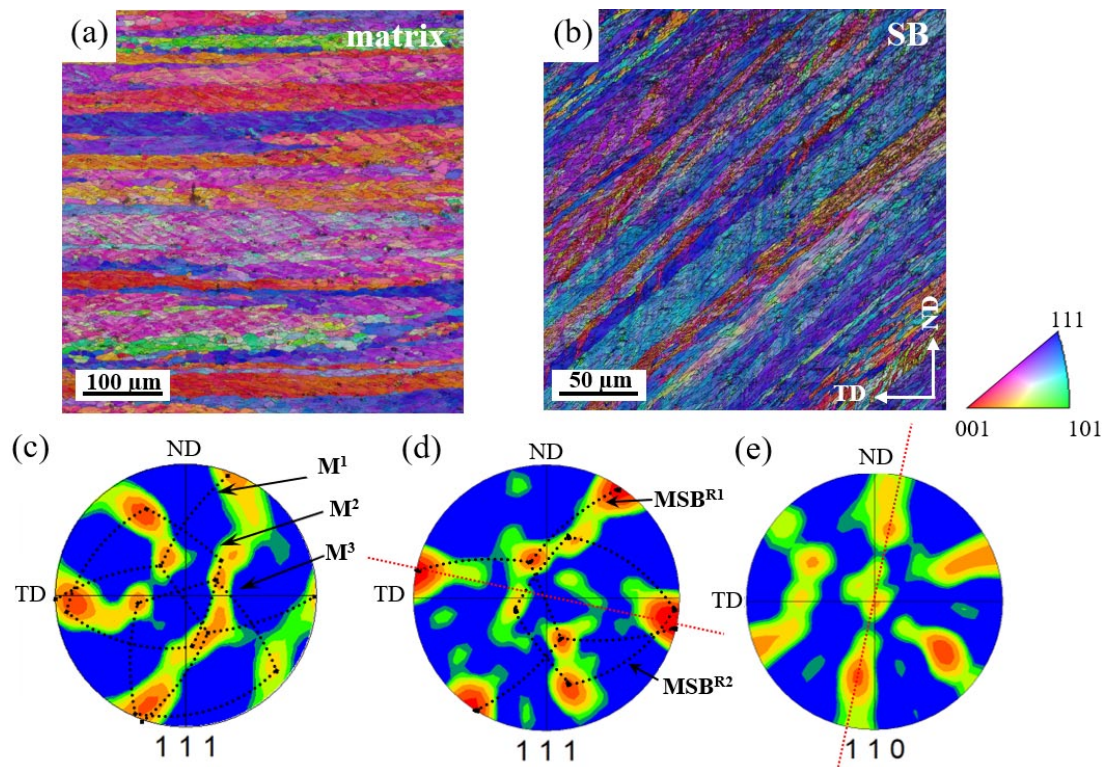

Fig. 4. Orientation changes resulting from macro-SB formation in AA1050 alloy. SEM/EBSD orientation maps measured in ND-TD section: (a) matrix and (b) macro-SB. (c) {111} pole figure with marked orientation groups identified in the matrix (M^1, M^2, M^3). (d) and (e) {111} and {011} pole figures showing texture from the macro-SB area (MSB^{R1} and MSB^{R2}). Black dotted lines mark main texture components present in matrix and macro-SB area, whereas red dotted lines reflect the traces of {111} planes and <110> directions corresponding to shear plane and shear direction, respectively. Maps are presented as a function of IPF and image quality factor. Step sizes of 200 nm and 150 nm, for the matrix and macro-SB area, respectively, were applied
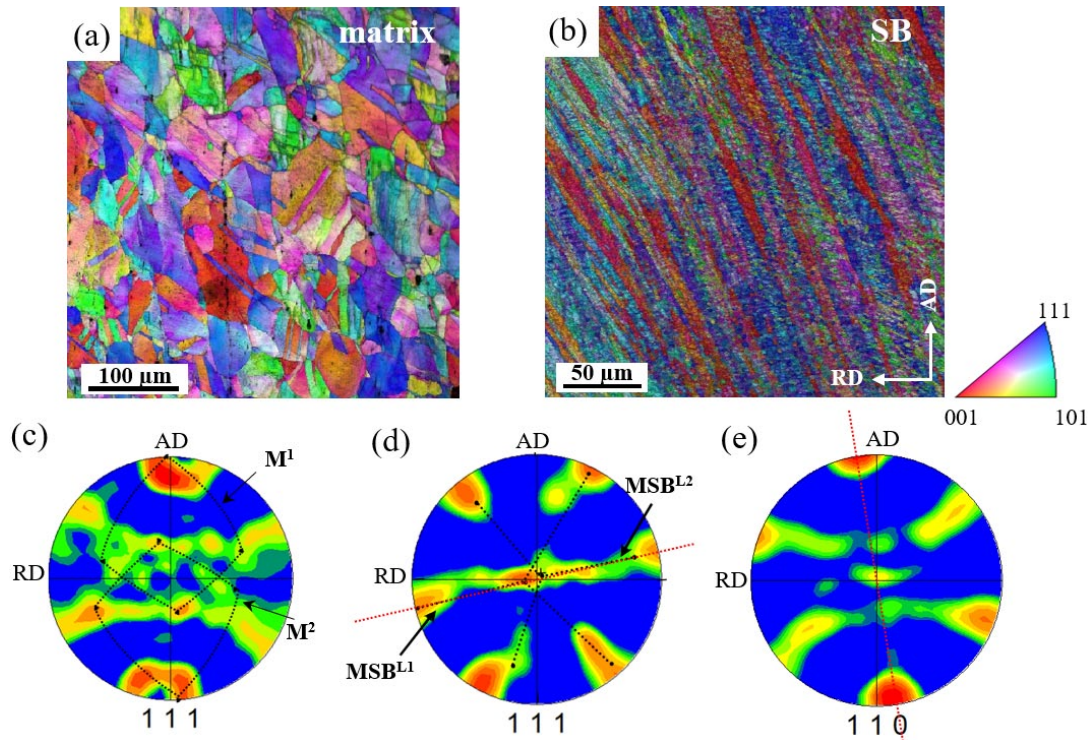
Fig. 5. Orientation changes due to macro- SB formation in Cu specimen. SEM/EBSD orientation map measured in AD-RD section: a) matrix and (b) macro- SB. (c) {111} pole figure with marked orientation groups identified in the matrix (M^1, M^2). (d) and (e) {111} and {011} pole figures showing texture from the macro- SB area (MSB^{L1} and MSB^{L2}). Black dotted lines mark the main texture components present in matrix and macro- SB area, whereas red dotted lines reflect the traces of {111} planes and <110> directions corresponding to the shear plane and shear direction, respectively. Maps are presented as a function of IPF and image quality factor. Step sizes of 400 nm and 200 nm for non-deformed matrix and macro- SB area, respectively, were applied
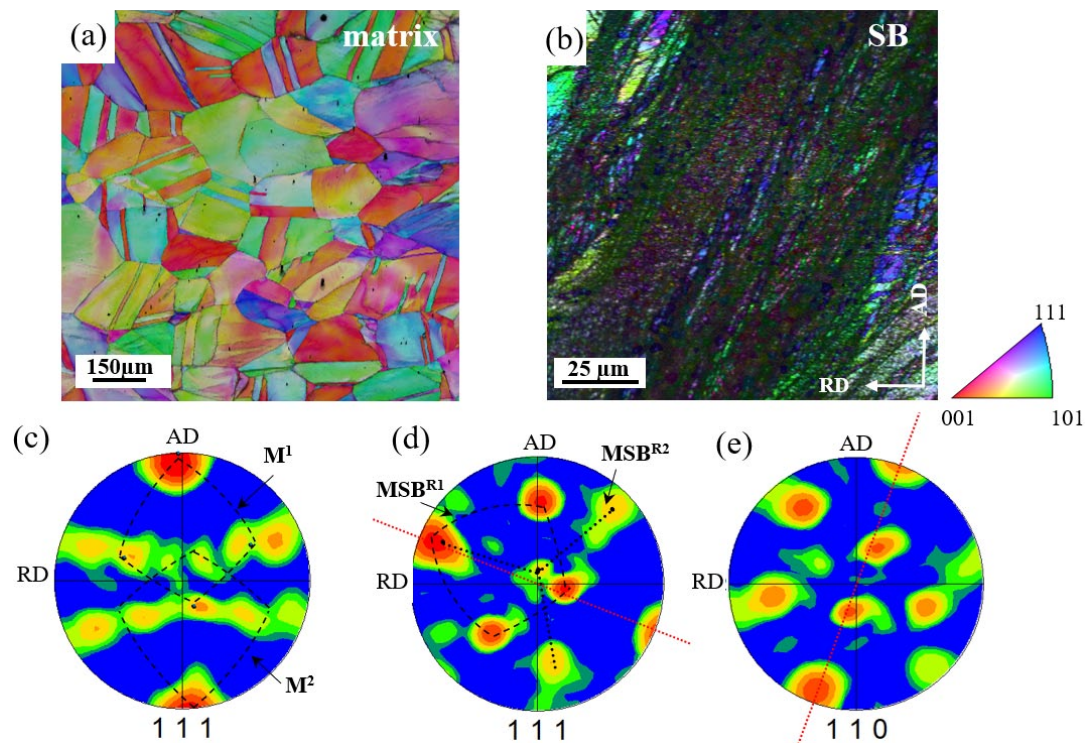

Fig. 6. Orientation changes due to macro- SB formation in Br specimen. SEM/EBSD orientation map measured in AD-RD section: a) matrix and (b) macro- SB. (c) {111} pole figure with marked orientation groups identified in the matrix (M^1, M^2). (d) and (e) {111} and {011} pole figures showing texture from the macro- SB area (MSB^{R1} and MSB^{R2}). Black dotted lines mark main texture components present in the matrix and macro- SB area, whereas red dotted lines reflect the traces of {111} planes and <110> directions corresponding to the shear plane and shear direction, respectively. Maps are presented as a function of IPF and image quality factor. Step sizes of 1 um and 200 nm for non-deformed matrix and macro- SB area, respectively were applied

as: (Br)M^1 – (1 3 4)[–1 –1 1] and (Br)M^2 – (9 8 2)[–6 5 7]. The appearance of macro- SB leads to (Fig. 6d-e) the texture components that may be described as: (Br) MSB^{R1} – (–2 3 –6)[–6 10 –3] and (Br) MSB^{R2} (9 5 8)[–3 7 –1].

Other experimental studies, e.g. [24,26] point out the fact that a deflection of the layered structure within narrow areas precedes SB formation and influences the textural changes. This study clarifies the complex mechanisms responsible for macro- SB formation (see section 3.6).

3.4. Strain hardening inside macro- SB. Nano-hardness measurements

Nanohardness measurements were carried out in each sample along a line scan across the shear band, starting and finishing in non (or less)-deformed matrix on both sides of the band. The part of the bands characterized by the largest shear strain localization was selected for measurements in each case. In other words, nanoindentation measurements were performed in the region where a most radical strengthening, with respect to the matrix, was demonstrated. In the case of Al and Cu specimens, the microstructure of the band interior is composed of strongly flattened grains. For the Br sample, characterized by low SFE, the interior of the band consists of highly dislocated, extremely small grains. This leads to a significant increase in nanohardness. The grains outside the band, especially those located in the axial areas of the specimens are non-deformed during impact, and no noticeable increase in the matrix nanohardness values is observed. The distribution of strain hardening (Fig. 7) shows that the nanohardness across macro- SB increases in the band area, and the maximum value corresponds to the core of the band, i.e. regions of the highest inclination of the flattened grains in Al and Cu or in ultra-fine-grained fragments of the band in the Br. In the core of the bands (Figs. 7a-c) the nanohardness is 1.6 times higher than in the surrounding non-deformed matrix.

3.5. Lattice re-orientation within macro- shear band

The optical micrographs and orientation maps in the area of the macro- SB of Figs. 3-7 revealed thin kink bands situated along the shear direction. The very first plastic instability within narrow areas by which the shear banding began, is similar to that observed earlier by TEM for the twinned structures of various fcc metals, e.g. [27]. The sense of this deflection could be described by a rotation that tends to decrease (in the analysed axial section) of the longer grain axis inclination with respect to the axial direction.

In this section, the details of the mechanisms responsible for the crystal lattice re-orientation in the sheared zone were examined. It is assumed here that the identification of rotation axes in the disorientation relation between the matrix and macro- SB is crucial in order to understand the mechanisms responsible for bands formation. During this process, texture components
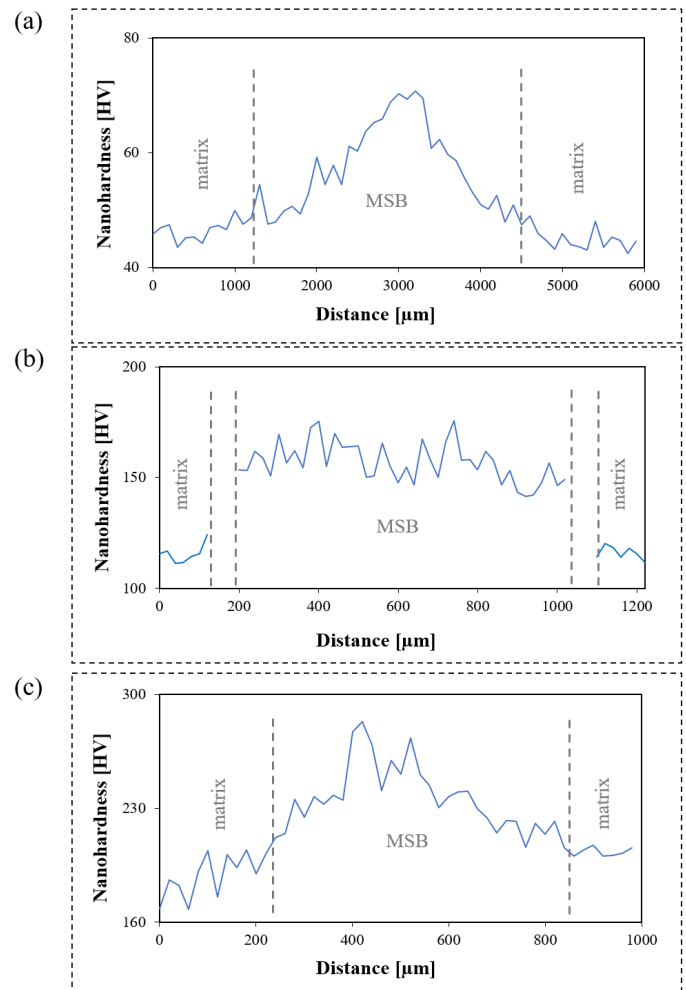

Fig. 7. Nanohardness measurements across macro- SB (MSB) in (a) Al, (b) Cu and (c) Br specimen showing the distribution of strain hardening. The measurement was carried out along the 'line scan' traversing the macro- SB. Dashed lines were applied in order to separate the macro- SB from the matrix area

of the non-deformed matrix are transformed into the groups of orientations observed inside the macro- SB *via* specific rotations. In all analysed crystal lattice rotations, leading to incorporation of the matrix into the macro- SB area result from the activity of specific {111}<011>-type slip system(s). This implies the occurrence of the rotation axis that is perpendicular to the normal of the active {111}-type slip plane and <110>-type slip direction. As a result of the activity of the {111}<110> systems, the matrix orientations undergo rotation around one of the <112>-type axis (single slip system) or <110>-type axis (double slip systems) resulting in the formation of main groups of texture components corresponding to the macro- SB area. Identified rotations for all metals are described as follow:

(a) Al

M^1(–1 1 0)[–1 –1 2] + 15° rotation around [–1 1 0] ⇨ MSB^{R1} (–1 1 0)[–1 –1 3]

M^2(0 4 –3)[–5 3 4] + 35° rotation around [–1 1 0] ⇨ MSB$^{R2(b)}$ (0 2 –3)[–5 3 2]

M^3(–1 1 0)[–5 –5 –2] + 35° rotation around [–210] ⇨ MSB$^{R2(a)}$ (–5 5 1)[–4 –3 –5]

(b) Cu

M^1(2 1 4)[–10 –8 7] + 20° rotation around [0 1 1] ⇨ MSB^{L1} (6 5 –1)[6 –7 1]

M^2(–1 3 –2)[–8 –6 –5] + 30° rotation around [0 –1 1] ⇨ MSB^{L2} (1 1 –1)[–6 7 1]

(c) Br

M^1(1 3 4)[–1 –1 1] – 20° rotation around [1 –2 –1] ⇨ MSB^{R1} (–2 3 –6)[–6 10 –3]

M^2(9 8 2)[–6 5 7] + 30° rotation around [–2 1 1] ⇨ MSB^{R2} (9 5 8)[–3 7 –1]

The schematic presentation of rotations transforming texture components of the matrix into the macro- SB texture components, for Al, Cu, and Br are shown in Figs. 8a-c, respectively. Identification of rotation axes and angles in disorientation relation between texture components of matrix and SB provides essential information needed to elucidate the transformation mechanisms. Analyses based on orientation changes resulting from the shear banding showed that groups of orientation identified in the matrix undergo different rotations – around <110>- or <112>-type axes. Those rotations are associated with the dominance of different active slip systems of {111}<011>-type.

The systematic crystal lattice rotation inside the macro- SB (during incorporation of the matrix into the SB area) is respon-

sible for changing the dominant slip system(s), which always occurs in agreement with the Schmid-Boas relationship. It is clear that the activity of new slip system(s) leads to a new rotation tendency of the crystal lattice as discussed in earlier works for *fcc* [24,28] and *bcc* [29,30] metals. These rotations are also crucial for slip propagation across the grain boundaries.

3.6. Slip propagation across the grain boundaries

Shear propagation through the grain boundaries is an important feature in the process of macro- SB formation. The situation is simple when the neighbouring flattened grains have a similar orientation, and one of the {111} planes (in each grain) coincides with the plane of maximum shear stresses. However, slip propagation also takes place in regions of quite different orientations. Nevertheless, from a crystallographic point of view, the existence of a {111} plane common for both areas is required.

The description of the crystal lattice rotation is also crucial to understanding the mechanism of slip propagation across the grain boundaries. Thus, more detailed EBSD measurements with a step size of 50 nm were carried out for the Br sample in regions of shear localization (Fig. 9) to determine the mechanism respon-
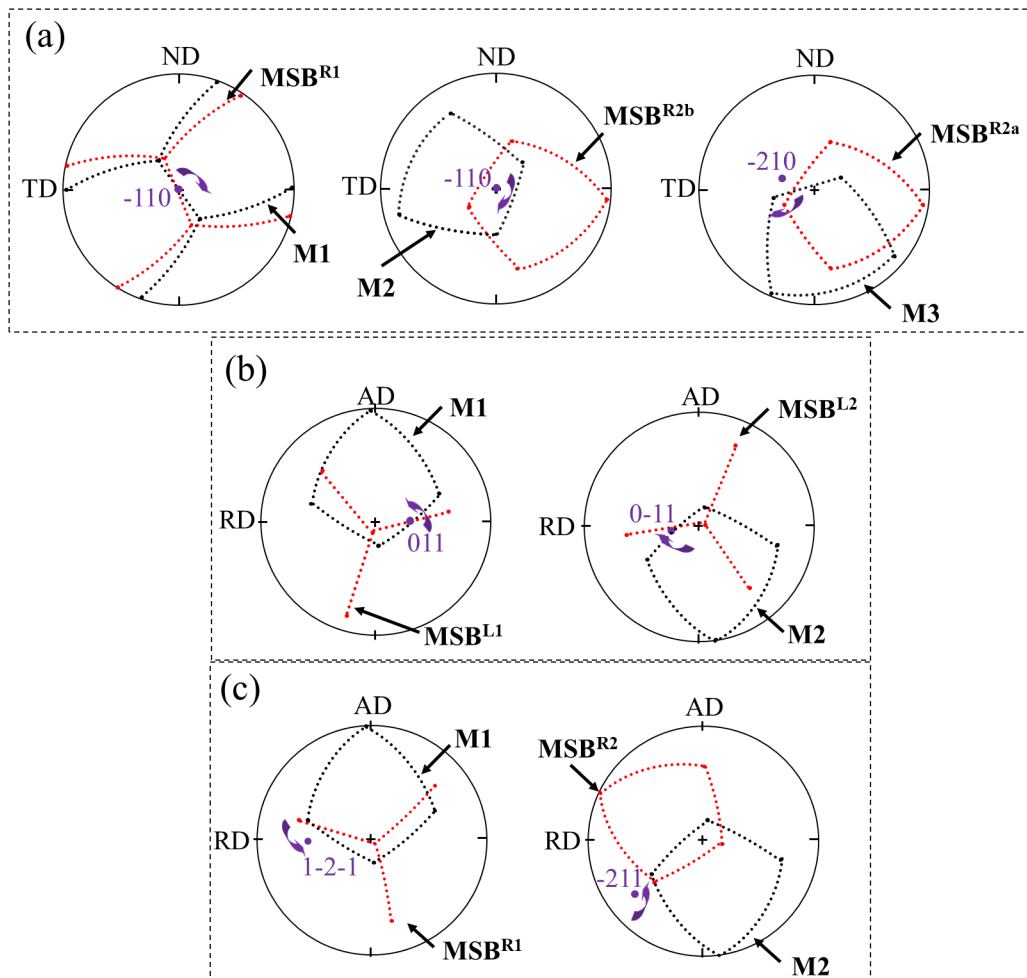

Fig. 8. Stereographic projections showing rotations of components identified in matrix into positions inside the macro- SB for: (a) Al, (b) Cu and (c) Br. The purple dot reflects the rotation axis. (M – texture component of the matrix, MSB – texture component identified in the sheared zone)
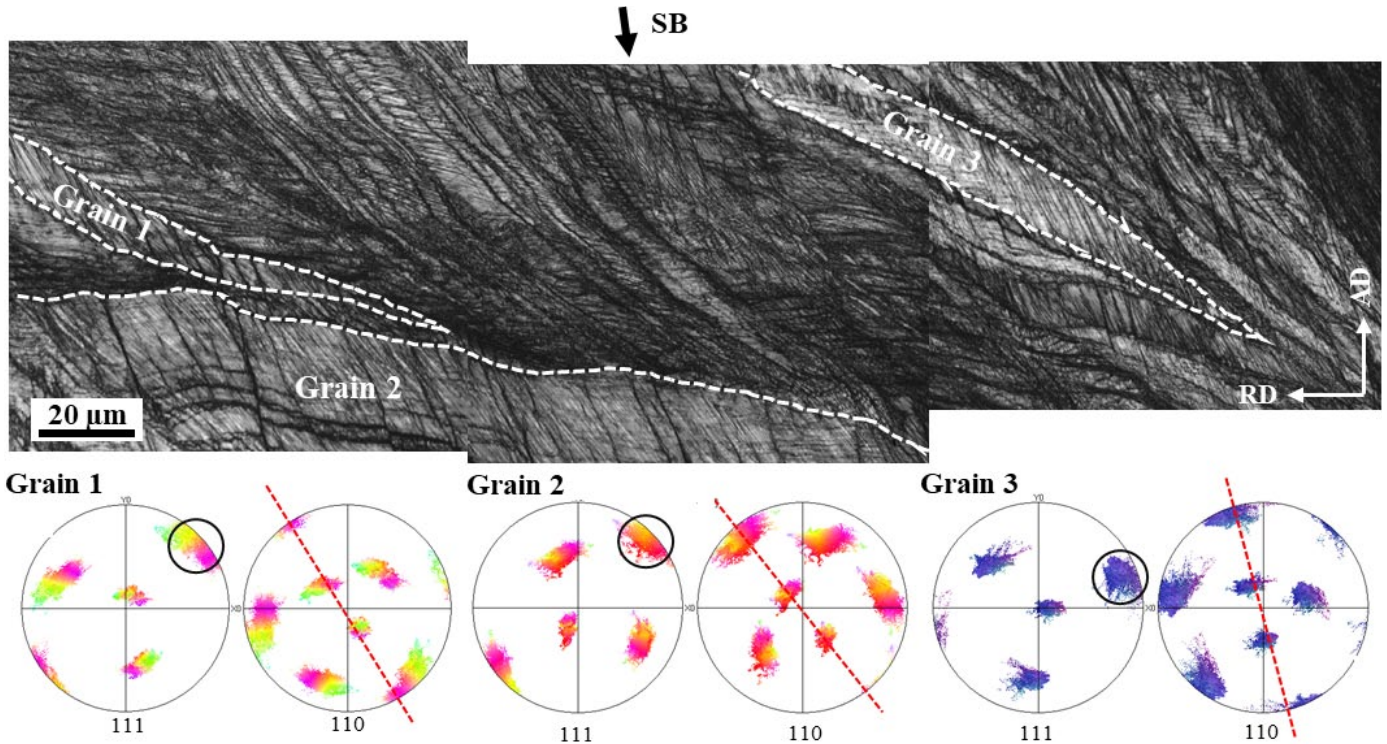
Fig. 9. Microstructure observed inside the area of macro- SB showing slip propagation across the grain boundaries (Grains 1-3). Orientation map displayed using image quality factor. The {111} pole figures showing the situation of important the {111} planes being nearly parallel to the shear plane (marked by black circles) and <110> directions being nearly parallel to the shear direction (marked by red dashed line). SEM/EBSD orientation measurements with step size of 100 nm

sible for the re-orientation of the initial crystal lattice in adjacent grains. Based on analysis of the slip traces and corresponding the {111} and {110} pole figures (showing orientations of matrix and macro- SB areas) it is deduced that the crystal lattice (as shown for grain 1, grain 2, and grain 3) rotated in such a way that traces of one of the {111} slip planes became nearly parallel to the direction of maximum shear, although the orientations of some grains were less or more different. Schematic presentation of an aspect concerning the macroscopically observed shear band despite slight misfit between {111} planes and <110> directions in the grains and shear band is shown in Fig. 10.

4. Conclusions

In the present study the mechanism of the microstructure and texture evolutions resulting from the macro- SB formation in aluminium, copper, and brass deformed at a strain rate of $560\ s^{-1}$ was clarified. With reference to the following research the most essential characteristics are:

(i)   for the applied strain rate all analysed metals show a tendency to strain localization. However, the morphology of the bands formed, and especially their thickness is strongly dependent on the metal analysed. In all cases, the areas of most intense shear are always located near both corners (near free surfaces) and propagate towards the centre of the sample.

(ii) As the SFE of the tested metals decreases, the strain localization tendency increases. In Al the formation of broad kink-type bands occurs while in Br relatively narrow regions of strongly localized strain are observed. Cu represents an intermediate behaviour.

(iii) The microstructure inside the SB and neighbouring severely deformed areas do not show any evidence of recrystallization, even in high stacking fault energy Al. Therefore, it is
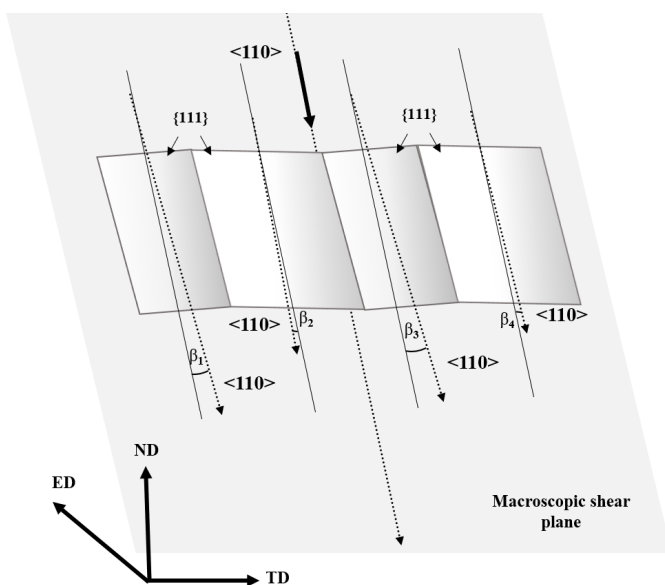

Fig. 10. Schematic representation of macroscopically observed SB plane composed of slightly disoriented planes in neighbouring grains. β – misfit angles between <110> direction and macroscopic shear direction

concluded that thermal softening or/and dynamic recrystallization does not play any important (if at all) role in the formation of SB under applied strain rate.

(iv) Morphological changes due to the occurrence of macro-SB are associated with the crystal lattice rotation in the grains situated within the sheared zone. The crystal lattice re-orientation inside particular grains tends to situate one of the {111} planes parallel to the macro- SB plane, while the <011> direction is parallel to the shear direction. This transformation coincides with the formation of new texture components different from those identified in the non-deformed matrix. However, in each case, the orientation relationship between the texture components of the matrix and the band interior can be described by a rotation around the <112> or <110> axis.

(v) Nanohardness within the centre of the macro- SB was ~ 60% higher than the as-received materials indicating a strong strain-hardening effect in the band region.

REFERENCES

[1] C. Zener, J.H. Hollomon, Effect of strain rate upon plastic flow of steel, J. Appl. Phys. **15**, 22-32 (1944).
DOI: https://doi.org/10.1063/1.1707363

[2] F. Adcock, The internal mechanism of cold work and recrystallization in cupro-nickel, J. Inst. Met. **27**, 73-105 (1922).

[3] R.C. Batra, Z.G. Wei, Shear bands due to heat flux prescribed at boundaries, Int. J. Plast. **22**, 1-15 (2006).
DOI: https://doi.org/10.1016/j.ijplas.2005.01.003

[4] T. Wright, Physics and Mathematics of Adiabatic Shear Bands, Appl. Mech. Rev. **56**, B41-B43 (2003).
DOI: https://doi.org/10.1115/1.1566401

[5] S. Osovski, D. Rittel, P. Landau, A. Venkert, Microstructural effects on adiabatic shear band formation, Scr. Mater. **66**, 9-12 (2012). DOI: https://doi.org/10.1016/j.scriptamat.2011.09.014

[6] V.F. Nesterenko, M.A. Meyers, J.C. LaSalvia, M.P. Bondar, Y.J. Chen, Y.L. Lukyanov, Shear localization and recrystallization in high-strain, high-strain-rate deformation of tantalum, Mater. Sci. Eng. A. **229**, 23-41 (1997).
DOI: https://doi.org/10.1016/s0921-5093(96)10847-9

[7] M.A. Meyers, G. Subhash, B.K. Kad, L. Prasad, Evolution of microstructure and shear-band formation in α-hcp titanium, Mech. Mater. **17**, 175-193 (1994).
DOI: https://doi.org/10.1016/0167-6636(94)90058-2

[8] M.A. Meyers, Y.B. Xu, Q. Xue, M.T. Pérez-Prado, T.R. McNelley, Microstructural evolution in adiabatic shear localization in stainless steel, Acta Mater. **51**, 1307-1325 (2003).
DOI: https://doi.org/10.1016/S1359-6454(02)00526-8

[9] F. Martinez, L.E. Murr, A. Ramirez, M.I. Lopez, S.M. Gaytan, Dynamic deformation and adiabatic shear microstructures associated with ballistic plug formation and fracture in Ti-6Al-4V targets, Mater. Sci. Eng. A. **454-455**, 581-589 (2007).
DOI: https://doi.org/10.1016/j.msea.2006.11.097

[10] D. Rittel, P. Landau, A. Venkert, Dynamic recrystallization as a potential cause for adiabatic shear failure, Phys. Rev. Lett. **101**, 2-5 (2008).
DOI: https://doi.org/10.1103/PhysRevLett.101.165501

[11] B. Huang, X. Miao, X. Luo, Y. Yang, Y. Zhang, Microstructure and texture evolution near the adiabatic shear band (ASB) in TC17 Titanium alloy with starting equiaxed microstructure studied by EBSD, Mater. Charact. **151**, 151-165 (2019).
DOI: https://doi.org/10.1016/j.matchar.2019.03.009.

[12] S. Zhu, Y. Guo, Q. Ruan, H. Chen, Y. Li, D. Fang, Formation of adiabatic shear band within Ti-6Al-4V: An in-situ study with high-speed photography and temperature measurement, Int. J. Mech. Sci. **171**, 105401 (2020).
DOI: https://doi.org/10.1016/j.ijmecsci.2019.105401

[13] Y.B. Xu, M.A. Meyers, Deformation, Phase Transformation and Recrystallization in the shear bands induced by high-strain rate loading in titanium and its allots, J. Mater. Sci. Technol. **22**, 737-746 (2006).
DOI: https://www.jmst.org/CN/Y2006/V22/I06/737

[14] J.A. Hines, K.S. Vecchio, S. Ahzi, A model for microstructure evolution in adiabatic shear bands, Metall. Mater. Trans. A Phys. Metall. Mater. Sci. **29**, 191-203 (1998).
DOI: https://doi.org/10.1007/s11661-998-0172-4

[15] D.R. Chichili, K.T. Ramesh, K.J. Hemker, The high-strain-rate response of alpha-titanium: Experiments, deformation mechanisms and modeling, Acta Mater. **46**, 1025-1043 (1998).
DOI: https://doi.org/10.1016/S1359-6454(97)00287-5

[16] D.K. Yang, P. Cizek, P.D. Hodgson, C.E. Wen, Microstructure evolution and nanograin formation during shear localization in cold-rolled titanium, Acta Mater. **58**, 4536-4548 (2010).
DOI: https://doi.org/10.1016/j.actamat.2010.05.007

[17] A.R. Shahan, A.K. Taheri, Adiabatic shear bands in titanium and titanium alloys: a critical review, Mater. Des. **14**, 243-250 (1993).
DOI: https://doi.org/10.1016/0261-3069(93)90078-A

[18] D.G. Lee, Y.G. Kim, D.H. Nam, S.M. Hur, S. Lee, Dynamic deformation behavior and ballistic performance of Ti-6Al-4V alloy containing fine α2 (Ti3Al) precipitates, Mater. Sci. Eng. A. **391**, 221-234 (2005).
DOI: https://doi.org/10.1016/j.msea.2004.08.076

[19] X. Liu, C. Tan, J. Zhang, F. Wang, H. Cai, Correlation of adiabatic shearing behavior with fracture in Ti-6Al-4V alloys with different microstructures, Int. J. Impact Eng. **36**, 1143-1149. (2009).
DOI: https://doi.org/10.1016/j.ijimpeng.2008.12.007

[20] S.C. Liao, J. Duffy, Adiabatic shear bands in a TI-6A1-4V titanium alloy, J. Mech. Phys. Solids. **46**, 2201-2231 (1998).
DOI: https://doi.org/10.1016/S0022-5096(98)00044-1

[21] D. Rittel, Z.G. Wang, M. Merzer, Adiabatic shear failure and dynamic stored energy of cold work, Phys. Rev. Lett. **96**, 1-4 (2006).
DOI: https://doi.org/10.1103/PhysRevLett.96.075502

[22] J. Duffy, Y.C. Chi, On the measurement of local strain and temperature during the formation of adiabatic shear bands, Mater. Sci. Eng. A. **157**, 195-210 (1992).
DOI: https://doi.org/10.1016/0921-5093(92)90026-W

[23] H. Paul, A. Morawiec, E. Bouzy, J.J. Fundenberger, A. Piatkowski, Brass-Type Shear Bands and their Influence on Texture Formation, Metall. Mater. Trans. A. **35A**, 3775-3786 (2004).
DOI: https://doi.org/10.1007/s11661-004-0283-5

[24] H. Paul, J.H. Driver, C. Maurice, A. Piatkowski, The role of shear banding on deformation texture in low stacking fault energy metals as characterized on model Ag crystals, Acta Mater. **55**, 575-588 (2007). DOI: https://doi.org/10.1016/j.actamat.2006.08.051

[25] H. Paul, A. Morawiec, J.H. Driver, E. Bouzy, On twinning and shear banding in a Cu-8 at.% Al alloy plane strain compressed at 77 K, Int. J. Plast. **25**, 1588-1608 (2009).
DOI: https://doi.org/10.1016/j.ijplas.2008.10.003

[26] C.S. Hong, N.R. Tao, X. Huang, K. Lu, Nucleation and thickening of shear bands in nano-scaletwin_matrix lamellae of a Cu-Al alloy processed by dynamic plastic deformation **33**, 379 (2010).

[27] H. Paul, J.H. Driver, C. Maurice, Z. Jasien, Crystallographic aspects of the early stages of recrystallisation in brass-type shear bands, Acta Mater. **50**, 4339-4355 (2002).

[28] A. Huot, R.A. Schwarzer, J.H. Driver, Texture of shear bands in Al-Mg 3% (AA5182) measured by BKD, Mater. Sci. Forum. **273-275**, 319-326 (1998).
DOI: https://doi.org/10.4028/www.scientific.net/msf.273-275.319

[29] D. Dorner, Y. Adachi, K. Tsuzaki, Periodic crystal lattice rotation in microband groups in a bcc metal, Scr. Mater. **57**, 775-778 (2007).
DOI: https://doi.org/10.1016/j.scriptamat.2007.06.048

[30] D. Dorner, S. Zaefferer, D. Raabe, Retention of the Goss orientation between microbands during cold rolling of an Fe3%Si single crystal, Acta Mater. **55**, 2519-2530 (2007).
DOI: https://doi.org/10.1016/j.actamat.2006.11.048